

University of Groningen

Identification of Receptor Binding to the Biomolecular Corona of Nanoparticles

Lara, Sandra; Alnasser, Fatima; Polo, Ester; Garry, David; Lo Giudice, Maria Cristina; Hristov, Delyan R; Rocks, Louise; Salvati, Anna; Yan, Yan; Dawson, Kenneth A

Published in:
Acs Nano

DOI:
[10.1021/acsnano.6b07933](https://doi.org/10.1021/acsnano.6b07933)

IMPORTANT NOTE: You are advised to consult the publisher's version (publisher's PDF) if you wish to cite from it. Please check the document version below.

Document Version
Publisher's PDF, also known as Version of record

Publication date:
2017

[Link to publication in University of Groningen/UMCG research database](#)

Citation for published version (APA):

Lara, S., Alnasser, F., Polo, E., Garry, D., Lo Giudice, M. C., Hristov, D. R., Rocks, L., Salvati, A., Yan, Y., & Dawson, K. A. (2017). Identification of Receptor Binding to the Biomolecular Corona of Nanoparticles. *Acs Nano*, 11(2), 1884-1893. <https://doi.org/10.1021/acsnano.6b07933>

Copyright

Other than for strictly personal use, it is not permitted to download or to forward/distribute the text or part of it without the consent of the author(s) and/or copyright holder(s), unless the work is under an open content license (like Creative Commons).

The publication may also be distributed here under the terms of Article 25fa of the Dutch Copyright Act, indicated by the "Taverne" license. More information can be found on the University of Groningen website: <https://www.rug.nl/library/open-access/self-archiving-pure/taverne-amendment>.

Take-down policy

If you believe that this document breaches copyright please contact us providing details, and we will remove access to the work immediately and investigate your claim.

Downloaded from the University of Groningen/UMCG research database (Pure): <http://www.rug.nl/research/portal>. For technical reasons the number of authors shown on this cover page is limited to 10 maximum.



Identification of Receptor Binding to the Biomolecular Corona of Nanoparticles

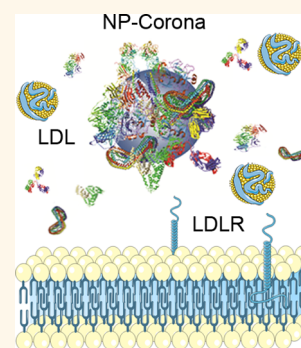
Sandra Lara,[†] Fatima Alnasser,[†] Ester Polo,[‡] David Garry, Maria Cristina Lo Giudice, Delyan R. Hristov, Louise Rocks, Anna Salvati,[#] Yan Yan,^{*‡} and Kenneth A. Dawson^{*}

Centre for BioNano Interactions, School of Chemistry and Chemical Biology, University College Dublin, Belfield, Dublin 4, Ireland

S Supporting Information

ABSTRACT: Biomolecules adsorbed on nanoparticles are known to confer a biological identity to nanoparticles, mediating the interactions with cells and biological barriers. However, how these molecules are presented on the particle surface in biological milieu remains unclear. The central aim of this study is to identify key protein recognition motifs and link them to specific cell-receptor interactions. Here, we employed an immuno-mapping technique to quantify epitope presentations of two major proteins in the serum corona, low-density lipoprotein and immunoglobulin G. Combining with a purpose-built receptor expression system, we show that both proteins present functional motifs to allow simultaneous recognition by low-density lipoprotein receptor and Fc-gamma receptor I of the corona. Our results suggest that the “labeling” of nanoparticles by biomolecular adsorption processes allows for multiple pathways in biological processes in which they may be “mistaken” for endogenous objects, such as lipoproteins, and exogenous ones, such as viral infections.

KEYWORDS: nanoparticle, biomolecular corona, receptor, low-density lipoprotein, epitope, internalization



When the nanoparticle (NP) surface comes in contact with a biological milieu, adsorption processes lead to a surface assembly of biomolecules derived from the environment, which has been termed “biomolecular corona”.^{1–3} It is now widely acknowledged that sufficiently long-lived (“hard corona”) biomolecular motifs presented at the surface would define how a NP first interacts with and is recognized by cells,^{4–11} and such interactions likely define many key biological outcomes (e.g., biodistribution, targeting, and immune responses).^{12–25} For example, apolipoproteins and immunoglobulins have been identified in the biomolecular corona of various types of NPs.³ Their presence has been suggested to promote active processes driven by receptors on the cells of the liver, which leads to liver accumulation of NPs that have commonly been observed for many types of NPs.²⁶ However, so far, the identities of the proteins that were tightly bound to an ensemble of NPs have been determined by mass spectrometry analysis of all the proteins extracted from the surface of all the NPs,^{3,27} which provides little information on how these proteins are organized, and their binding motifs are presented. The lack of molecular details of corona conformation has hindered us from meaningfully determining “what the cell sees”.^{28,29} Approaches using immuno-probes for detection of specific protein epitopes presented outward on the NP surface have recently been developed.^{30,31} These allow us to seek direct microscopic molecular connections between the biomolecular corona and specific receptors.

Here, we present a systematic method to advance such hypotheses by direct investigation of NP–receptor interactions

in biological milieu. As one example, a protein corona derived from human serum on 100 nm silica (SiO₂) NPs was chosen as a model. Given the abundance of low-density lipoprotein (LDL) and immunoglobulin G (IgG) in the corona characterized by proteomics analysis, their orientation on the corona was probed by mapping the epitopes of apolipoprotein B-100 (ApoB-100) for the LDL and Fc region for IgG. Approximately, 60 ApoB-100 binding sites and 180 Fc binding sites per particle were detected in the biomolecular corona derived from 50% human serum by using a fluorescence reporter binder (quantum dots (QDs) functionalized with antibodies). Subsequently, we developed a receptor fusion protein expression system to study specific recognition by the LDL receptor (LDLR) and Fc-gamma receptor I (FcγRI) in appropriate biological milieu. We recognize the difficulty of maintaining effective receptor interactions with soluble receptor fragments for most receptors of interest. Thus, the purpose of these receptor fusion systems is to host relevant receptors, in a manner that retains binding capacity, without seeking to re-engineer the host cell, and all of the complexity and uncertainty this entails. As such, the readout of a specific recognition of a biomolecular corona by receptors is an increase of NP uptake when cells express the receptors in comparison to being devoid of the receptors. The presence of free proteins in normal serum

Received: November 25, 2016

Accepted: January 23, 2017

Published: January 23, 2017

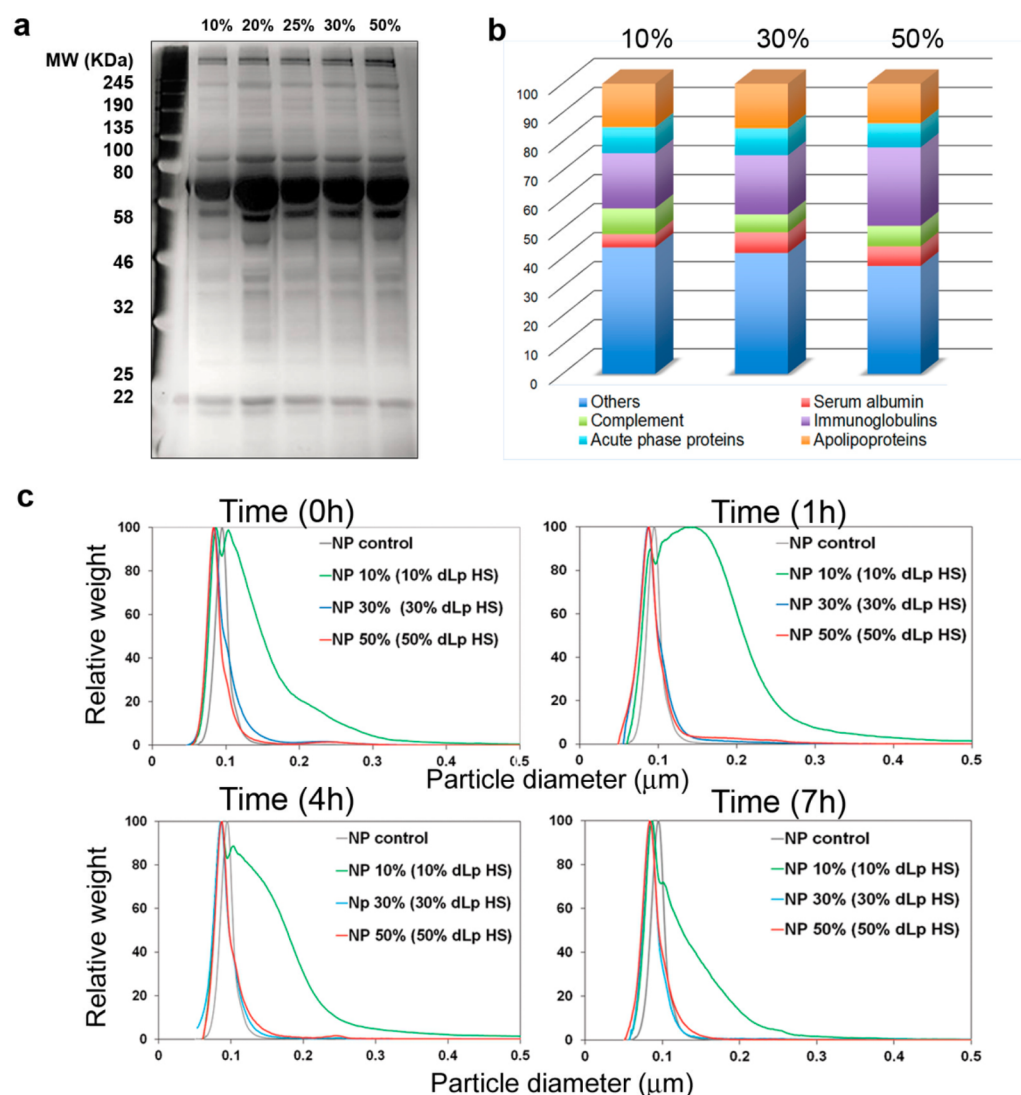


Figure 1. Physicochemical characterization of serum corona on 100 nm SiO₂ NPs. (a) SDS-PAGE of protein coronas recovered from SiO₂ NPs following incubation with human serum at various concentrations. (b) Distribution of protein groups in human serum corona analyzed by LC-MS/MS. The proteins on the SDS-PAGE were identified by LC-MS/MS after in-gel tryptic digestion. The abundance of protein groups is expressed as protein mass percentage of the total corona proteins. (c) Differential centrifugal sedimentation analysis of NP dispersions in delipidized human serum for various time periods: NPs with hard coronas formed in 10, 30, and 50% of human serum were redispersed in 10, 30, and 50% delipidized human serum for 1, 4, and 7 h, respectively.

is likely to decrease the detection window, as the competition between free proteins and NP-adsorbed protein recognition motifs for specific membrane receptors would only occur in receptor-expressing cells. Therefore, NP uptake was carried out in human serum that was depleted from the free proteins that are binding ligands for a given receptor in this study. Our data have shown that the uptake of NPs is significantly increased in the cells with greatly elevated expression of either LDLR or FcγRI, suggesting that the specific recognition of the corona by both receptors is coexistent. The specificity of the receptor recognition was further confirmed by competition binding of free ligands with increasing concentrations. Taken together, this study illustrates that the biomolecular corona of NPs retains multiple binding motifs, which can be specifically recognized by different receptors potentially with diverse receptor–ligand affinity.

RESULTS AND DISCUSSION

Physicochemical Characterization of NPs in Biological Milieu. For many particle–serum systems, the strongly bound hard corona is sufficiently stable so that it is possible to connect the surface expression of surface-adsorbed protein epitopes to the cell biological interactions.³² Thus, we first expose 100 nm SiO₂ NPs to different percentages of human serum (*i.e.*, 10, 30, and 50%) and isolate the hard corona–NP complexes by centrifugation. Using denatured polyacrylamide gel electrophoresis (SDS-PAGE) and mass spectrometry, the irreversibly bound hard corona proteins on SiO₂ NPs were separated, identified, and analyzed (Figure 1a,b and Table S1). Lipoproteins and immunoglobulins were found to be abundant in all coronas with more than 10 and 20% of the total corona proteins, respectively. Key examples include LDL and IgG. LDL particles (20–30 nm in diameter), containing several thousand cholesterol, phospholipid, and triglyceride molecules, possess a single copy of ApoB-100, which interacts with the

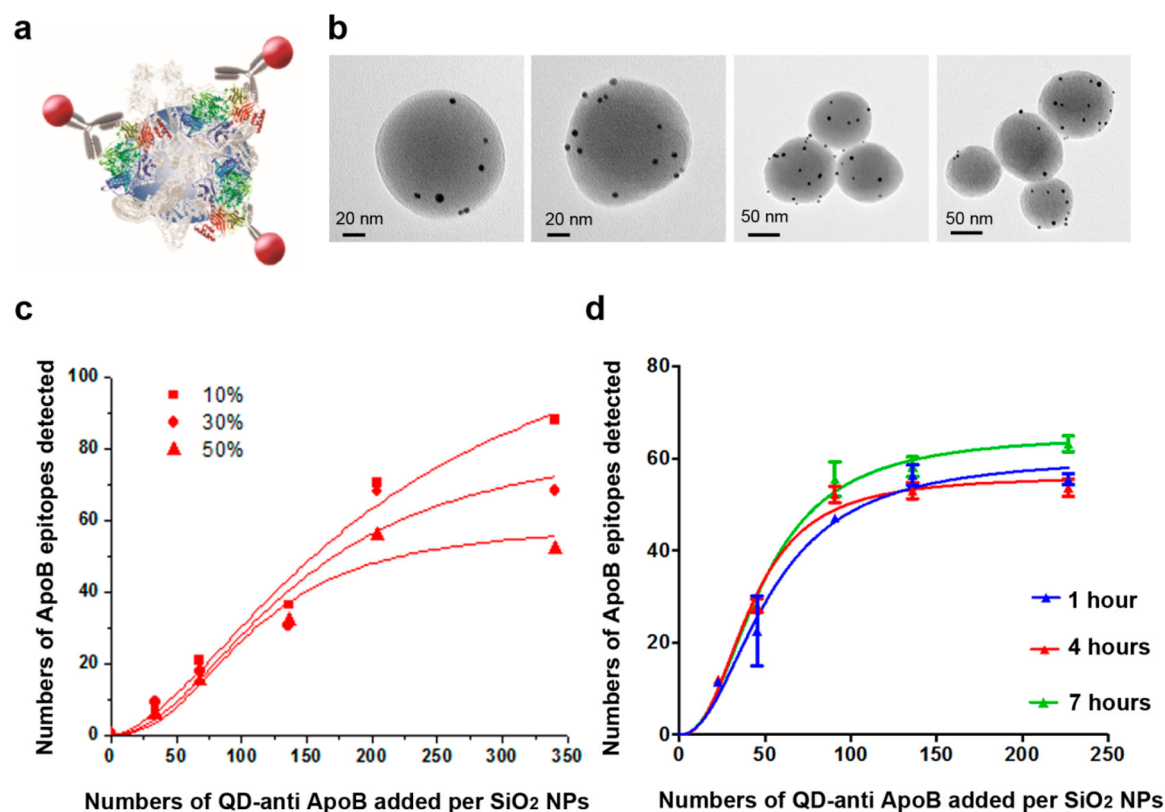


Figure 2. Epitope mapping of ApoB-100 on the serum corona of 100 nm SiO₂ NPs. (a) Schematic representation of epitope mapping of ApoB-100 on the protein corona of SiO₂ NPs by 5 nm immuno-gold NPs conjugated with antibodies recognizing the ApoB-100 epitope. (b) Electron micrographs of ApoB-100 epitopes on SiO₂ NPs with a corona formed in 50% of human serum and subsequently incubated in 50% of delipidized serum for 4 h. (c,d) Quantification of ApoB-100 epitope on corona-NP complexes using immuno-QDs. (c) Corona-NP complexes were formed in 10, 30, and 50% human serum and subsequently redispersed in PBS for 1 h. The immuno-QD labeling was performed with the corona-NP dispersion in PBS. (d) Corona-NP complexes were formed in 50% human serum and subsequently redispersed in 50% delipidized human serum and incubated for 1, 4, and 7 h. The immuno-QDs were obtained with the corona-NP dispersion in 50% delipidized serum. Data represent the mean and standard deviation of three independent replicates.

LDLR.^{33–35} IgG, the most abundant type of antibody in circulatory system, consists of four peptide chains. Through the Fc region, IgG binds to a family of Fc-gamma receptors (including FcγRI) to mediate various immunological responses (e.g., activation of phagocytes and antibody-dependent cell-mediated cytotoxicity).³⁶ It is unclear if the higher amount of IgG is a consequence of nonspecific adsorption or secondary recognition of disrupted corona proteins by blood-borne antibodies.

Next, we sought to characterize their physicochemical properties in appropriate biological milieu. In general, for nanomaterials, the role of the milieu is critical and cell origin must be matched to the appropriate biological fluid to ensure fidelity of protein recognition.²⁹ For the following studies, we intend to use LDL as an example to illustrate the concept. First, we redispersed the corona-NP complexes in serum depleted of the lipoproteins (see lipoprotein depletion in Figure S1), as it is important to examine the particle uptake in the absence of free LDL to avoid competitive binding. Subsequently, we characterized the same NP-corona dispersions that were used for cell uptake studies with varied serum concentrations and incubation times. Time-resolved differential centrifugal sedimentation (DCS) analyses showed that in 10% delipidized serum there is a degree of instability of the dispersion over some hours, but for both 30 and 50% serum concentrations, the

dispersions are stable over the lifetime of typical cell uptake experiments (Figure 1c).

For such stable well-defined dispersions, we can analyze the epitopes presented at the surface of nanoparticle-corona complexes using immuno-labeling approaches that have the sensitivity to detect 2–4 epitopes per nanoparticle.³⁷ Monoclonal antibody (mAb) that recognizes the region of AA 97–526 of ApoB-100, close to the LDLR recognition site, was conjugated to a gold NP (4.5 nm, Figure S2a,b) or a QD (4 nm, Figure S2c,d). After incubation with immuno-gold NP-mAbs, the ApoB-100 epitopes were visualized by transmission electron microscopy (TEM) (Figure 2a,b). To quantitatively detect the epitope presentation in the same conditions as the NPs are exposed to the cells, we employed a QD-mAb mapping technique.³⁸ First, we examined the titration of ApoB-100 epitopes on the coronas formed by exposure of NPs to 10, 30, and 50% human serum at 37 °C for 1 h and redispersed in PBS. Different numbers of ApoB-100 epitopes were detected on the different coronas, with the 10% serum corona showing the highest number of ApoB-100 epitopes (Figure 2c). Subsequently, we performed the titration curve of QD-mAb probes with the corona-NP complexes that were formed in 50% serum and then redispersed in 50% delipidized serum for 1, 4, and 7 h. The three titration curves showed significant overlapping, suggesting that the number of epitopes remains relatively constant throughout the time period (Figure 2d). It is

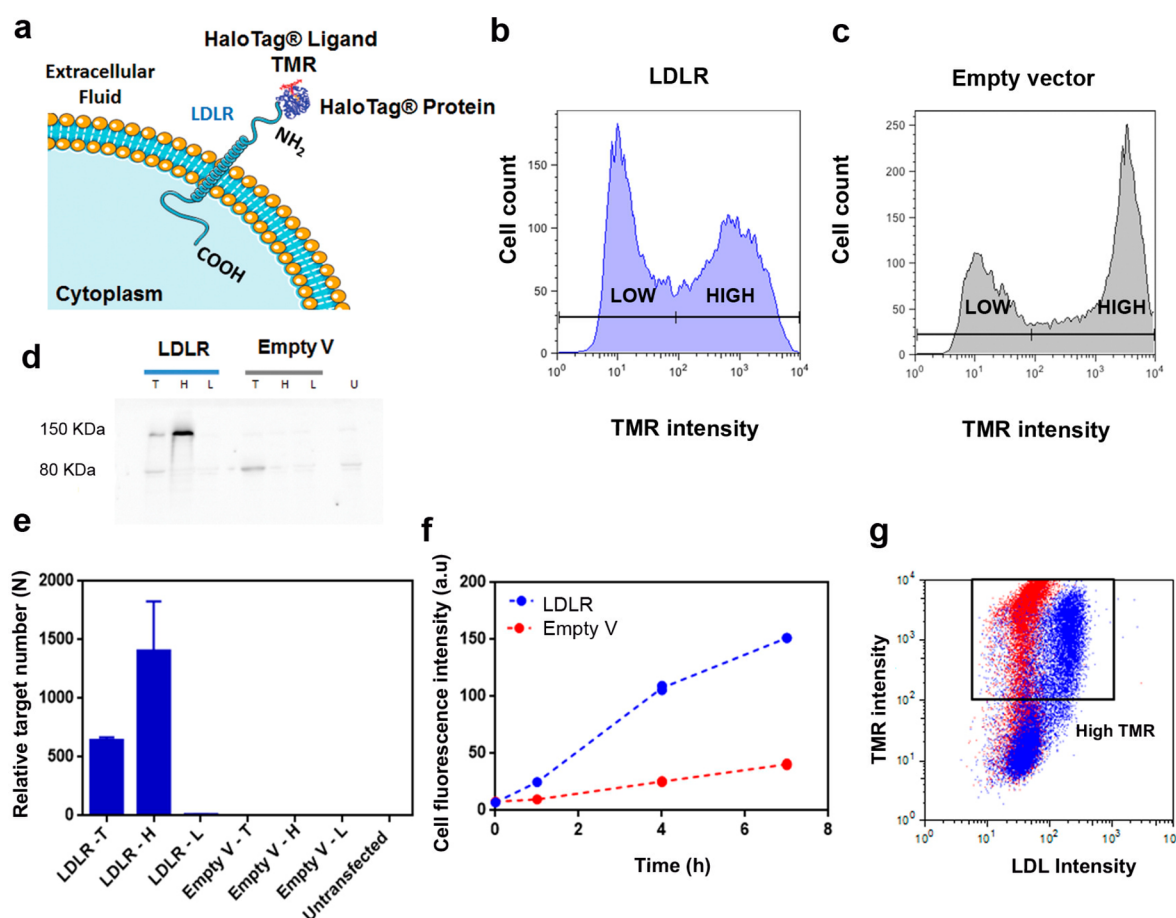


Figure 3. Expression of human LDLR in HEK-293T cells. (a) Scheme of LDLR fused with a HaloTag protein at its N-terminus. The HaloTag protein forms a covalent bond with a fluorescent HaloTag ligand, TMR. (b) Expression of LDLR–HaloTag fusion protein in cells transfected with a LDLR vector after incubation with TMR measured by flow cytometry. (c) Expression of a HaloTag protein in cells transfected with an empty vector after incubation with TMR measured by flow cytometry. Cells were sorted to two populations (high and low) based on the TMR intensity. (d) Western blot analysis of LDLR expression (MW 95 kDa) probed by using an anti-LDLR monoclonal antibody. (e) Quantification of LDLR mRNA level by RT-qPCR after transfection with a LDLR vector in the total cell population (LDLR-T), sorted high TMR (LDLR-H) and low TMR (LDLR-L) subpopulations, as well as equivalent samples after transfection with an empty vector. The data are shown as the mean \pm standard deviation of triplicates. (f) Uptake kinetics of BODIPY-LDL ($5 \mu\text{g mL}^{-1}$) by cells transfected with a LDLR vector in 50% human serum analyzed by flow cytometry. Data represent the median fluorescence intensity of transfected cells (high TMR subpopulation) performed in duplicates. At least 15 000 cells were analyzed in each repeat. (g) Example of a 2D plot of BODIPY-LDL and TMR intensity (4 h time point). High TMR subpopulation is highlighted in the square. Blue: LDLR-transfected cells. Red: Empty vector transfected cells.

noted that the number of ApoB-100 epitopes reached a plateau of 60 with an increased ratio of QD–mAb probes to SiO₂ NPs (Figure 2d), which is similar to the number of ApoB-100 epitopes quantified for the same hard corona (*i.e.*, 50% serum corona) redispersed in PBS for 1 h (Figure 2c). This further supports the notion that the corona–NP complexes are stable. Figure 2 establishes that the potential recognition fragment of ApoB-100 is indeed extensively presented at the NP surface in biological milieu. The question is if it is still recognizable by the relevant receptor, LDLR.

Target Cells for Study of NP–Receptor Interactions. A straightforward way of detecting specific uptake pathways is to compare the NP uptake kinetics curves (for example, using time-resolved flow cytometry) of two identical populations of cells, one of which has many less (or more) receptors of a given type than the other population of cells with other key receptors that can interact with the NPs remaining unchanged.³⁹ Silencing RNA (siRNA) of the receptors of interest could be used to determine recognition of NPs by decreasing the

receptor expression. To explore the siRNA approach, we transfected LDLR siRNA to decrease the endogenous expression of LDLR in A549 human lung epithelial cells (Figure S3). By comparison of particle uptake between LDLR siRNA and scrambled siRNA-transfected A549 cells, it is confirmed that LDLR down-regulation leads to a decrease of NP uptake (Figure S4). It is worth noting that LDL exists in different forms in serum (*e.g.*, oxidized LDL), and besides LDLR, it can be recognized by other receptors, including LOX-1, CD36, and Toll-like receptor 4 (TLR-4).^{40,41} A closer analysis has shown that transfection with LDLR siRNA in A549 cells concurrently increased LOX-1 expression (Figure S3), suggesting a high degree of co-regulation of the genes. Given the cross-talking between the receptors, it suggests that comparison of reference and silenced cells may not be a reliable approach in this case.

Alternatively, in this study, we have developed a receptor-tag fusion protein expression system that can “host” a range of target receptors in HEK-293T cells (Figure 3). These cells have

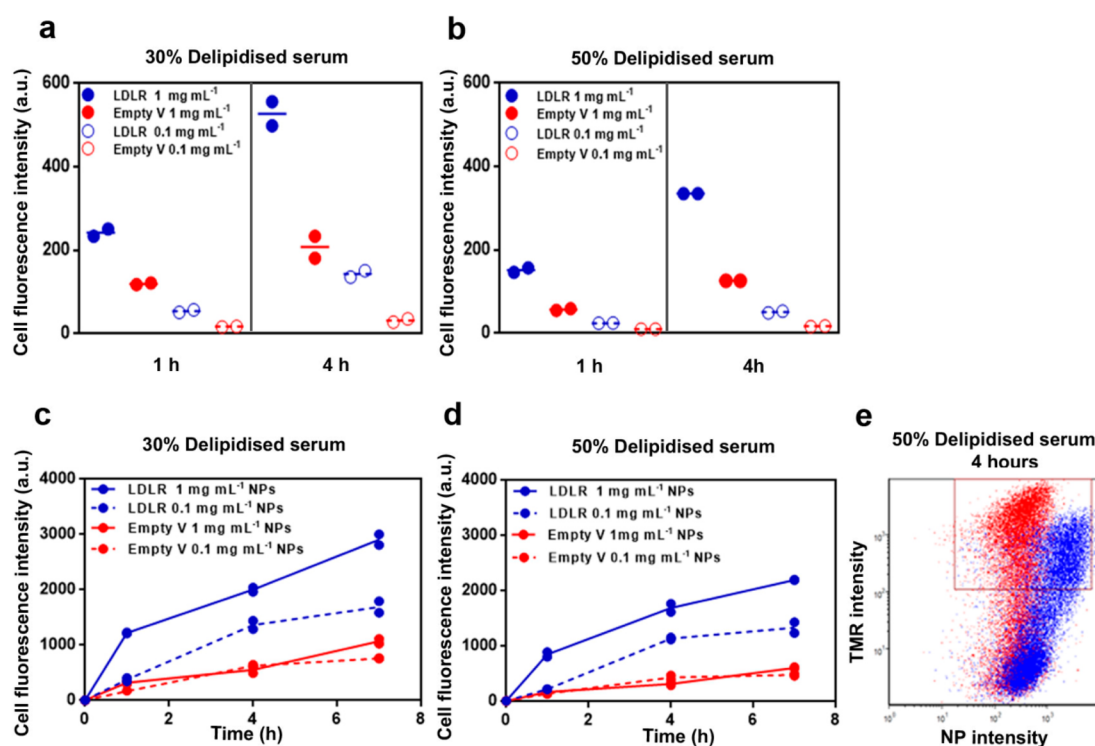


Figure 4. Membrane adhesion and uptake of human serum corona-SiO₂ NP complexes in delipidized serum. (a,b) Membrane adhesion of corona-NP complexes in delipidized serum. Cells were exposed to corona-NP complexes in 30% (a) and 50% (b) delipidized serum at 4 °C for 1 and 4 h, followed incubation at 37 °C for 30 min. Data represent the median fluorescence intensity of transfected cells (high TMR subpopulation) performed in duplicates. At least 15 000 cells in each repeat were measured by flow cytometry. (c,d) Uptake of corona-NP complexes in delipidized serum. Cells were exposed to corona-NP complexes in 30% (c) and 50% (d) delipidized serum at 37 °C for 1, 4, and 7 h. Data represent the median fluorescence intensity of transfected cells (high TMR subpopulation) performed in duplicates. At least 15 000 cells were analyzed in each repeat. (e) Example of a 2D plot of NP and TMR intensity (50% delipidized serum, 4 h incubation). High TMR subpopulation is highlighted in the square. Blue: LDLR-transfected cells. Red: Empty vector transfected cells.

a very low endogenous expression level of LDLR, and transfection of LDLR does not appear to co-regulate at the gene (or protein) level within the relevant receptor clusters (Figure S5). Crucially, the receptor is fused with the HaloTag, which can then be labeled with a fluorescent HaloTag ligand, TMR (Figure 3a). This dye labeling serves as an intrinsic measure of receptor expression on a cell-by-cell basis using flow cytometry. As it is shown in Figure 3b,c, the expression of the LDLR-HaloTag fusion protein and HaloTag protein alone varied significantly between cells. Some cells failed to be transfected (the left-most low TMR subpopulation in Figure 3b,c) even with optimization of the transfection (Figure S6). Hence, we note that if the complete ensemble of cells after transfection is used (both parts of the populations in Figure 3b), it becomes difficult to identify NP-receptor recognition. The correlation between receptor expression level and NP uptake is critical for confirming the specific corona epitope-receptor recognition, given the heterogeneity in both receptor expression and particle surface presentation. Thus, cell subpopulations (*i.e.*, high TMR and low TMR) were sorted based on TMR intensity. Western blot (Figure 3d) and RT-qPCR (Figure 3e) both confirm that TMR levels can be used as a proxy for receptor expression.

To confirm functionality of the expressed LDLR, we examined the uptake of fluorescently labeled LDL in the high TMR subpopulations (*i.e.*, transfected cells). A 4-fold increase in the fluorescence of cells transfected with LDLR was observed compared to that of the empty vector transfected cells (Figure 3f). It is noted that the LDL uptake was independent of LDLR

expression level in the high TMR subpopulation (Figure 3g), suggesting that average numbers of expressed plasma membrane receptors are high and functional.

In Situ Interactions of NPs with LDLR. Using the above-mentioned LDLR-tag fusion protein expression system, we examined the cell membrane adhesion and uptake of NP-corona in delipidized serum. For the membrane adhesion experiment, the cells were incubated with NP-corona complexes at 4 °C for 1 and 4 h followed by extensive washes to remove unbound NPs and subsequently chased in NP-free media at 37 °C for 30 min. For the uptake experiment, the cells were continuously incubated with NP-corona complexes at 37 °C for various time intervals. As shown in Figure 4, significantly increased membrane adhesion and uptake by LDLR-transfected cells (*i.e.*, the high TMR subpopulation) was observed in all dispersions in comparison to cells transfected with an empty vector. It is also noted that at higher NP concentration (1 mg mL⁻¹) and a higher serum concentration (50% delipidized serum), the specific uptake of NPs by LDLR was maximized, as the baseline uptake (*i.e.*, uptake in cells transfected with empty vector) was minimized due to other uptake pathways suppressed by serum competition (Figure 4c,d). Under such conditions, the scatter plot (4 h time point as an example) showed a high correlation between LDLR expression and NP uptake on a cell-by-cell basis in the transfected cells (highlighted in the inset box of Figure 4e).

To further establish the specificity of the ApoB-100 interaction, we carried out competition uptake experiments (50% delipidized serum, 4 h) for conditions identical to those

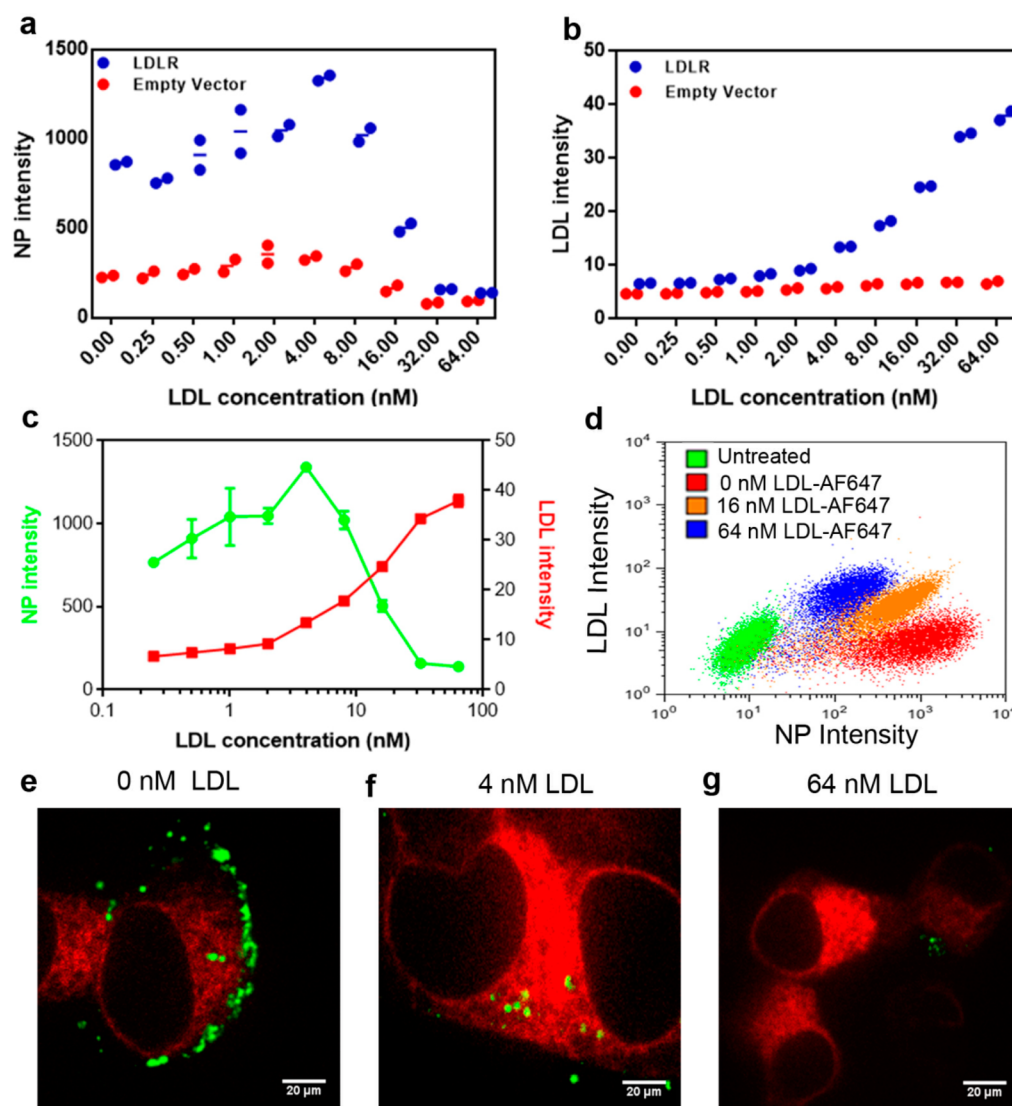


Figure 5. Competitive uptake of human serum corona-SiO₂ NP complexes by LDL in delipidized serum. Cells were incubated with corona-NP complexes (labeled with FITC, 0.1 mg mL⁻¹) and increasing concentrations of AF647-LDL (0 to 64 nM) in 50% delipidized serum at 37 °C for 4 h. NP (a) and LDL (b) uptake was measured by flow cytometry. Data are the median fluorescence intensity of transfected cells (high TMR subpopulation) performed in duplicates. (c) Uptake of NPs competed with LDL in LDLR-transfected cells. Data are shown as the median of cell fluorescence intensity of transfected cells \pm standard deviation of duplicates. (d) Two-dimensional scatter plots show uptake of NPs and LDL in untreated cells, LDLR-transfected cells in the absence and presence of AF647-LDL. Confocal images of NP uptake (in green) in LDLR-transfected cells (stained with TMR in red) (e) in the absence of LDL and in the presence of (f) 4 nM LDL and (g) 64 nM LDL.

in Figure 4c,d but in the presence of increasing concentrations of fluorescently labeled LDL (Figure 5). Then we can simultaneously measure the uptake of NPs and LDL and find that at around 16 nM LDL there is quite a sharp accumulated displacement-type transition in which predominantly NP uptake crosses over to predominantly LDL uptake (Figure 5a–c). The scatter plot of LDL and NP fluorescence intensity indicates that cells that interact most strongly with LDL also have the highest NP uptake, suggesting involvement of the same receptor (Figure 5d). Confocal microscopy images have also shown a progressive competitive uptake of NPs with an increase of free LDL (Figure 5e–g).

We remark that the specific recognition of the serum corona by LDLR can be reproduced from independent experiments using the SiO₂ NPs made in house and commercially sourced with the same surface and similar size (Figure S7). Collectively these observations set a high standard of reproducibility, which

we find to be broadly applicable to a number of other particle and receptor systems.

Concurrent Interactions of NPs with the FcγRI Receptor. To provide a different perspective, we present (in less detail) analogous data for FcγRI, a receptor that recognizes the Fc regions of IgGs, and a member of the important receptor superfamily that promotes phagocytosis of (for example) opsonized particles and infectious agents.^{42,43} The presentation of Fc epitopes in the biomolecular corona was quantified using anti-IgG (Fc) QD labeling. It was shown around 180 Fc epitopes were detected in the corona (Figure 6b), which is higher than the ApoB-100 epitopes (around 60 epitopes) and is consistent with more abundant immunoglobulins found in the corona than in apolipoproteins (Figure 1b).

Next, we employed the receptor-tag fusion expression system to examine the specific recognition by the FcγRI receptor. As shown in Figure 6d, FcγRI-transfected cells exhibited increased

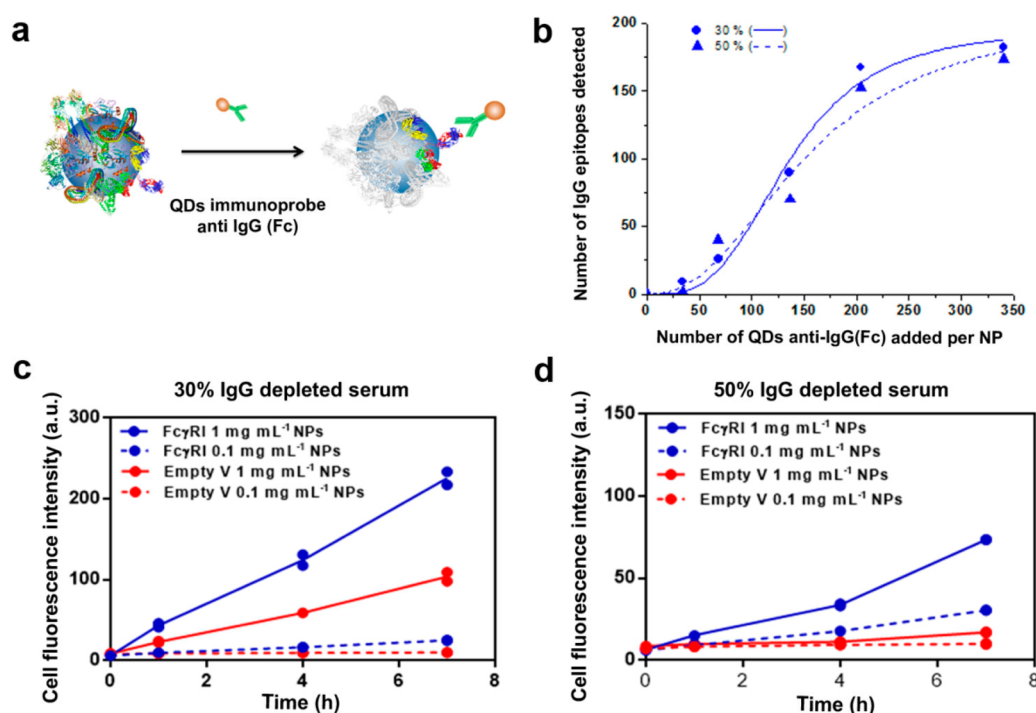


Figure 6. Epitope mapping of IgG (Fc) in the serum corona of SiO₂ NPs and their cellular recognition by the FcγRI receptor in IgG-depleted serum. (a) Schematic representation of epitope mapping of the Fc region on the corona of SiO₂ NPs in IgG-depleted serum by immuno-QD labeling. (b) Quantification of the Fc epitope on corona-NP complexes using immuno-QDs. The corona-NP complexes were formed in 30 and 50% human serum and subsequently redispersed in PBS for 1 h. The immuno-QD labeling was measured with the corona-NP dispersion in PBS using fluorescence spectroscopy. (c,d) Uptake of corona-NP complexes in IgG-depleted serum. Cells were exposed to corona-NP complexes in 30% (c) and 50% (d) IgG-depleted serum at 37 °C for 1, 4, and 7 h. Data represent the median fluorescence intensity of transfected cells (high TMR subpopulation) performed in duplicates. At least 15 000 cells were analyzed in each repeat.

uptake of particles compared to that of untransfected cells in both 30 and 50% IgG-depleted serum, suggesting that FcγRI plays a role in particle recognition. The overall uptake scale in IgG-depleted serum is much smaller than that in LDL-depleted serum, despite the fact that abundance of IgG and LDL in the corona and the affinity of free IgG and LDL to FcγRI and LDLR, respectively, are comparable. Also, uptake using dual depleted serum (*i.e.*, lipid- and IgG-depleted) shows little difference between FcγRI-transfected and control cells (Figure S8), possibly suggesting a much larger interaction between particles and LDLR.⁴⁴ The reasons for the apparently less effective interaction of IgG are not clear, and we do not believe it prudent to overinterpret this observation. We do note, however, that the typical affinities of recognition sites on NPs may be quite unrelated to that of the native protein and could also vary significantly on a particle-by-particle basis. Such questions go far beyond the current studies and may require additional tools.

CONCLUSIONS

Fundamentally, the size of NPs moves them into the range where many intrinsic biological messages are passed and processed. Since adsorption of biomolecules on the NPs “labels” them with endogenous molecules, this potentially allows for ubiquitous “accidental” involvement in biological processing. Thus, NPs may be “mistaken” for endogenous (*e.g.*, lipoproteins) or commonly occurring exogenous objects (*e.g.*, viruses), potentially manifested in the nature of their clearance and other outcomes. In this study, by using LDL and IgG as examples, we have demonstrated that adsorbed proteins on

SiO₂ NPs can present functional epitopes to allow the specific recognition of receptors. While this study has been focused on two types of receptors, we have been able to express a wide spectrum of receptors using such a system (*e.g.*, scavenger receptor class A member 1, scavenger receptor class B member 1, stabilin-1, stabilin-2, and the other 10 receptors that are abundant in the liver) and consider the platform will be of broad significance for NP-receptor recognition studies.

It would also be important to note that these are only the first steps. There are still several significant limitations that are a consequence of the complexity of NP-cell interactions. For example, NP-protein complexes are highly heterogeneous systems in which we have recognized major contributions from predominant, not rare, NP subpopulations. In addition, multivalent interactions between receptors and NPs have often been speculated upon, but the synergies between receptors at the interface of NPs are poorly studied, and such effects are yet to be understood. Still, we now have systematic mapping and cellular tools that allow us to connect the real nature of the bio-nano interface to cellular interactions. This brings closer the microscopic connection between a particle and its biological impact, with all the promise that could hold for predicting and controlling biological outcomes.

METHODS

Materials. Fluorescein isothiocyanate (FITC)-labeled 100 nm SiO₂ NPs with a plain surface were synthesized at the CBNI as described previously.⁴⁵ The 100 nm green fluorescent, plain surface SiO₂ NPs (PSi-G0.1) were purchased from KISKER-BIOTECH (see characterization in Figure S9). Anti-LDL receptor antibody [1B10H10] (ab204941), anti-FcγRI antibody [3D3] (ab140779), and anti-mouse

IgG H+L (HRP) (ab6728) were purchased from Abcam. Anti-ApoB-100 sc-13538, anti-ApoA-I sc-13549, and anti-ApoE sc-13521 were purchased from SantaCruz Biotech. BODIPY-LDL (L3483), CD64/FCGR1A antibody (10.1) MA1-10270, goat anti-mouse IgG (H+L) secondary antibody, and Alexa Fluor 488 conjugate (A11029) were ordered from Thermo Fisher. Human serum was purchased from BIOCHROM. Delipidized human serum was purchased from SERALAB. IgG-depleted human serum was purchased from INNOV-RESEARCH. The plasmid vectors for expression of LDLR (FHC01394) and FcγRI (FHC03501) were purchased from KAZUSA DNA Research Institute. Propan-2-ol (P/7507/5) was purchased from Fisher Chemical. LDLR silencer select siRNA (s224006), silencer select negative control no. 1 (439064), and oligofectamine transfection reagent (12252011) were purchased from Thermo Fisher. Skimmed milk powder (70166), sodium dodecyl sulfate (L3771), glycine (G8898), ammonium persulfate (A3678), Trizma base (T1503), Tween 20 (P1379), ethylenediaminetetraacetic acid disodium salt dihydrate, EDTA (E4884), *N,N,N',N'*-tetramethylethylenediamine (T9281), select agar (A5054), acrylamide/bisacrylamide, 40% solution (A7802), ampicillin (A9393), DL-dithiothreitol (D5545), ethanol (32294-2), methanol (24229-2), 3-mercaptopropionic acid (M5801), cadmium chloride (202908), hydrogen tetrachloroaurate(III) (S20918), 4-aminophenyl β -D-galactopyranoside (A9545), sodium borohydride (S9125), *N*-(3-(dimethylamino)propyl)-*N'*-ethylcarbodiimide hydrochloride (E6383), *N*-hydroxysulfosuccinimide sodium salt (S6485), and methoxypolyethylene glycol amine (07964) were purchased from Sigma-Aldrich and used as received. Color plus prestained protein ladder, broad range (10–230 kDa) (P7711S) and blue loading buffer for SDS-PAGE were purchased from New England Bio-Laboratories (cat. no. B77035). PVC calibration standard for DCS measurements 483 nm (PS000483) was ordered from Analytik Ltd. BCA protein assay kit (23227) and RIPA buffer (89901) were ordered from Thermo Scientific. Propan-2-ol (P/7507/5) was purchased from Fisher Chemical. Tellurium, 99.8%, powder (315990250) was purchased from Acros Organics.

NP Characterization. SiO₂ NPs used in this study were characterized by dynamic light scattering and DCS to ensure the stability of the dispersion (Figure S9). To obtain the hard corona, 1 mg of 100 nm SiO₂ NPs was incubated with 1 mL of 10% human serum (5 mg mL⁻¹ protein concentration), 30% human serum (15 mg mL⁻¹ protein concentration), or 50% human serum (25 mg mL⁻¹ protein concentration) at 37 °C for 1 h on a shaker followed by centrifugation at 16 000 rcf for 20 min. After centrifugation, the pellet was redispersed and washed with phosphate-buffered saline (PBS, pH 7.4) three times. The protein corona was analyzed by SDS-PAGE and LC-MS/MS following the protocol described previously.³ The corona–NP complexes were redispersed in 10, 30, or 50% delipidized human serum and were characterized by DCS at different time points before the epitope mapping analysis. The NP dispersions were characterized by DCS using a CPS disc centrifuge DC24000. For SiO₂ NPs, a 8–24% sucrose density gradient (suitable for the nanoparticle density range used) prepared in relevant solvents (PBS, pH 7.4) was used with a disk speed of 20 000 rpm. The particles were measured between 0.001 and 1 μ m, with each measurement being calibrated with a PVC standard with a nominal size of 483 nm (Analytik Ltd.).

Epitope Mapping. The synthesis of small gold NPs (5 nm) was performed following the procedure reported previously.⁴⁶ In order to functionalize the gold NPs with antibodies, the citrate of the NP surface was exchanged by *O*-(2-carboxyethyl)-*O'*-(2-mercaptoethyl)-heptaethylene glycol (SH-PEG (7)-COOH, MW = 458.56 g/mol). Briefly, 50 mL of gold NPs after synthesis was incubated overnight, under continuous stirring, with SDS (0.03%), NaOH (25 mM), and an equivalent amount of SH-PEG (7)-COOH to obtain 5000 chains per NP. The carboxylated gold NPs were washed three times and concentrated with centrifugal filter units (10 000 MWCO). The gold NPs were characterized by DCS and EM. The synthesis of mercaptopropionic acid (MPA)-protected CdTe QDs was performed following the procedure reported by Penadés *et al.*⁴⁷ The QDs were purified by precipitation with acetone. Finally, the QDs were separated

by centrifugation and dialyzed 48 h against PBS buffer. The QD particles were characterized by DCS and fluorescence spectroscopy.

The CdTe–MPA QDs and gold NPs were functionalized with antibodies: 1 mL of NP suspension (3.3 nmol) was mixed with 0.4 mg of EDC and 0.8 mg of sulfo-NHS in PBS buffer pH 7.4, and the mixture was incubated at 37 °C for 30 min. The activated NP solution was applied to a PD-10 column using 10 mM PBS pH 7.4 as the exchange buffer. Then 0.6 nmol of IgG antibody was added to 1 nmol of NPs, and the mixture was stirred at 37 °C for 1 h. Subsequently, the activated carboxylic groups were blocked with 5 mg of 4-aminophenyl β -D-galactopyranoside, and the mixture was incubated overnight in a final volume of 1.5 mL. NPs conjugated with antibodies (650 nm) were stored at 4 °C.

For the immuno-gold labeling, mAb–gold NPs (5 nm) in excess were added to a given number of corona–NP complexes. After the incubation, the NPs were collected by centrifugation at 16 000 rcf and washed with PBS and Milli-Q water five times each to remove unbound mAb–gold NPs. Then the samples were prepared for TEM as described previously.³⁰ Three hundred SiO₂ NPs were analyzed for immuno-gold label counting by a FEI Tecnai G2 20 Twin TEM operating at an acceleration voltage of 200 kV. For the QD–mAb labeling, different amounts of immuno-QDs in PBS (up to final concentration at 500 nM) were added to the NP–corona complexes (final concentration at 1 mg mL⁻¹) under constant agitation for 1 h at 37 °C. Subsequently, the samples were centrifuged at 16 000 rcf and redispersed in fresh PBS twice to remove the unbound QD–mAbs. The interaction between the immuno-QDs and the corona was studied using steady-state fluorescence spectroscopy as described previously.³¹

Cell Culture. Human embryonic kidney (HEK-293T) cells (ATCC CRL-3216) and human adenocarcinomic alveolar basal epithelial A549 cells (ATCC-CCL-185) were purchased from ATCC, which were authenticated by the ATCC. HEK-293T cells were cultured in DMEM, high glucose, Glutamax (GIBCO), supplemented with 10% fetal bovine serum (FBS, GIBCO) in a humidified chamber at 37 °C under 5% CO₂. A549 cells were cultured in MEM (GIBCO), supplemented with 10% FBS at 37 °C and 5% CO₂. Cells were grown in their preferred environment and passed three times a week, as they approached 70–80% surface coverage. The cells were routinely tested for mycoplasma contamination by using the MycoAlert assay kit (Cambrex Bio Science, Nottingham, UK).

RNA Extraction and RT-qPCR. RNA was extracted using an InvitrapSpin cell RNA mini kit from Strattec (0711). The amount of RNA was quantified by NanoDrop, and the cDNA was obtained by reverse transcription. Quantitative PCR was performed with the cDNA of each population of interest and the specific primers for each receptor. Comparative CT method ($\Delta\Delta$ CT) was used to perform the calculations. The CT (cycle threshold) of the receptor of interest was normalized with the CT of the β -actin to obtain its Δ CT. The values of Δ CT of the receptors were further normalized with the Δ CT of the control cells (*i.e.*, untransfected cells), the result of which generated the final data set ($\Delta\Delta$ CT).

Western Blot. Proteins separated by SDS-PAGE were transferred to a PVDF membrane using a mini-PROTEAN tetra trans-blot module under a constant voltage of 100 V for 1 h. Membranes were then incubated at room temperature for 1 h in blocking solution of 5% skimmed milk in TBS-TWEEN (150 mM NaCl, 10 mM Tris-HCl, 0.1% Tween, pH 7.5). Afterward, the membrane was incubated overnight at 4 °C with the antibodies of interest in blocking solution and washed for 1 h in TBS-TWEEN. The blot was incubated at room temperature for 1 h with 1:2000 of anti-goat HRP in blocking solution and washed for 1 h in TBS-TWEEN. The membrane was incubated for 1 min in an ECL Western blotting substrate mix and visualized in a Syngene G: BOX imaging system.

Silencing of LDLR Expression in A549 Cells. Seventeen thousand cells were seeded in 24-well plates (Greiner) and incubated for 24 h before silencing of LDLR. Cells were then transfected with LDLR siRNA or scrambled siRNA using oligofectamine reagent according to the manufacturer's instructions and incubated for 72 h.

Transfection of HEK-293T Cells. HEK-293T cells were plated 24 h before transfection at a density of 104 000 cells in each well into a

12-well plate (Cellstar Greiner bio-one) in 1 mL of complete DMEM Glutamax (GIBCO) medium supplemented with 10% FBS. After 24 h, cells were transfected using a FuGENE 6 (Promega)-to-DNA ratio of 3.5:1 for LDLR and 3:1 for FcγRI. Plasmid DNA ($0.02 \mu\text{g } \mu\text{L}^{-1}$) was added to a sterile tube containing opti-MEM medium (GIBCO). FuGENE 6 reagent was added to the solution and mixed carefully by pipetting 15 times. The solution was incubated at room temperature for 10 min. Next, $50 \mu\text{L}$ was then gently added dropwise onto each well and incubated for 24 h at 37°C and 5% CO_2 .

Cellular Uptake of NPs. To expose the cells to the NPs, after 24 h of the transfection, cells were washed for at least 30 min in serum-free DMEM. The medium was then replaced with the freshly prepared NP dispersions. Experiments were performed by exposing the cells to the NP dispersions at 0.1 or 1 mg mL^{-1} at 37°C and 5% CO_2 for 1, 4, and 7 h. Cells then were washed with 1 mL per well of completed DMEM Glutamax supplemented with 10% FBS. One-fifth of the volume was replaced with TMR HaloTag ligand at a concentration of 200 nM in completed DMEM Glutamax and incubated at 37°C , 5% CO_2 for 15 min. The cells were washed with completed DMEM Glutamax once and PBS twice and harvested after trypsinization. Cell pellets were redispersed in completed DMEM Glutamax and placed on ice. Cell fluorescence intensity was measured using a CyAn ADP (Beckman Coulter flow cytometer). Results are reported as the median of cell fluorescence intensity of transfected cells (high TMR subpopulation). At least 15 000 cells were analyzed in each sample.

ASSOCIATED CONTENT

Supporting Information

The Supporting Information is available free of charge on the ACS Publications website at DOI: 10.1021/acsnano.6b07933.

Table of proteins identified in the human serum corona of SiO_2 by LC-MS/MS; Western blot confirming the depletion of lipids in human serum; physical characterization of gold NPs and QDs for antibody conjugation; receptor expression in LDLR-silenced A549 cells; NP uptake in LDLR-silenced A549 cells; receptor mRNA levels in LDLR-transfected HEK-293T cells; optimization of transfection; reproducibility of corona-NP uptake in LDLR-transfected HEK-293T cells; uptake of corona-NPs in lipid- and IgG-depleted serum; and physicochemical characterization of NPs used in this study (PDF)

AUTHOR INFORMATION

Corresponding Authors

*E-mail: yan.yan@cbni.ucd.ie.

*E-mail: kenneth.a.dawson@cbni.ucd.ie.

ORCID

Ester Polo: 0000-0001-8870-5280

Yan Yan: 0000-0003-2938-4063

Present Address

[#](A.S.) Groningen Research Institute of Pharmacy, University of Groningen, A. Deusinglaan 1, 9713AV Groningen, The Netherlands

Author Contributions

[†]S.L. and F.A. contributed equally to this work.

Notes

The authors declare no competing financial interest.

ACKNOWLEDGMENTS

This work was supported by the Science Foundation Ireland (SFI) Principal Investigator Award (Agreement No. 12/IA/1422) and Starting Investigator Researcher Grant (Agreement

No. 15/SIRG/3423). S.L., E.P., D.G., M.C.L.G., and L.R. acknowledge the Science Foundation Ireland (SFI, 12/IA/1422). F.A. acknowledges the Saudi Arabia Scholarship Program (the Ministry of Education, Saudi Arabia). D.R.H. acknowledges EU FP7 FutureNanoNeeds project (Agreement No. 604602). Experimental method development was also supported by the EU FP7 QualityNano research infrastructure (Agreement No. 2621633) and the EU FP7-PEOPLE-2012-IAPP Marie Curie NanoClassifier (Agreement No.324519). The Conway Institute Flow Cytometry, Biological Imaging Suite, and Proteomics facilities at the University College Dublin are also acknowledged. The authors are grateful for assistance from Alfonso Blanco (flow cytometry), Matthias Wilm (proteomics), Kanlaya Prapainop (receptor experiments), Rong Miao (receptor experiments), Andrzej Pitek (receptor experiments), Filippo Bertoli (imaging), and Andre Potti (serum depletion).

REFERENCES

- (1) Cedervall, T.; Lynch, I.; Lindman, S.; Berggård, T.; Thulin, E.; Nilsson, H.; Dawson, K. A.; Linse, S. Understanding the Nanoparticle-Protein Corona Using Methods to Quantify Exchange Rates and Affinities of Proteins for Nanoparticles. *Proc. Natl. Acad. Sci. U. S. A.* **2007**, *104*, 2050–2055.
- (2) Monopoli, M. P.; Åberg, C.; Salvati, A.; Dawson, K. A. Biomolecular Coronas Provide the Biological Identity of Nanosized materials. *Nat. Nanotechnol.* **2012**, *7*, 779–786.
- (3) Monopoli, M. P.; Walczyk, D.; Campbell, A.; Elia, G.; Lynch, I.; Baldelli Bombelli, F.; Dawson, K. A. Physical-Chemical Aspects of Protein Corona: Relevance to *in Vitro* and *in Vivo* Biological Impacts of Nanoparticles. *J. Am. Chem. Soc.* **2011**, *133*, 2525–34.
- (4) Tenzer, S.; Docter, D.; Kuharev, J.; Musyanovych, A.; Fetz, V.; Hecht, R.; Schlenk, F.; Fischer, D.; Kiouptsi, K.; Reinhardt, C.; Landfester, K.; Schild, H.; Maskos, M.; Knauer, S. K.; Stauber, R. H. Rapid Formation of Plasma Protein Corona Critically Affects Nanoparticle Pathophysiology. *Nat. Nanotechnol.* **2013**, *8*, 772–781.
- (5) Schöttler, S.; Becker, G.; Winzen, S.; Steinbach, T.; Mohr, K.; Landfester, K.; Mailänder, V.; Wurm, F. R. Protein Adsorption Is Required for Stealth Effect of Poly(ethylene glycol)- and Poly-(phosphoester)-Coated Nanocarriers. *Nat. Nanotechnol.* **2016**, *11*, 372–377.
- (6) Deng, Z. J.; Liang, M.; Monteiro, M.; Toth, I.; Minchin, R. F. Nanoparticle-Induced Unfolding of Fibrinogen Promotes Mac-1 Receptor Activation and Inflammation. *Nat. Nanotechnol.* **2011**, *6*, 39–44.
- (7) Rocker, C.; Potzl, M.; Zhang, F.; Parak, W. J.; Nienhaus, G. U. A Quantitative Fluorescence Study of Protein Monolayer Formation on Colloidal Nanoparticles. *Nat. Nanotechnol.* **2009**, *4*, 577–580.
- (8) Mortimer, G. M.; Butcher, N. J.; Musumeci, A. W.; Deng, Z. J.; Martin, D. J.; Minchin, R. F. Cryptic Epitopes of Albumin Determine Mononuclear Phagocyte System Clearance of Nanomaterials. *ACS Nano* **2014**, *8*, 3357–3366.
- (9) Walkey, C. D.; Olsen, J. B.; Guo, H.; Emili, A.; Chan, W. C. Nanoparticle Size and Surface Chemistry Determine Serum Protein Adsorption and Macrophage Uptake. *J. Am. Chem. Soc.* **2012**, *134*, 2139–2147.
- (10) Del Pino, P.; Pelaz, B.; Zhang, Q.; Maffre, P.; Nienhaus, G. U.; Parak, W. J. Protein Corona Formation around Nanoparticles-from the Past to the Future. *Mater. Horiz.* **2014**, *1*, 301–313.
- (11) Pelaz, B.; Del Pino, P.; Maffre, P.; Hartmann, R.; Gallego, M.; Rivera-Fernandez, S.; De la Fuente, J. M.; Nienhaus, G. U.; Parak, W. J. Surface Functionalization of Nanoparticles with Polyethylene Glycol: Effects on Protein Adsorption and Cellular Uptake. *ACS Nano* **2015**, *9*, 6996–7008.
- (12) He, X.; Zhang, Z.; Liu, J.; Ma, Y.; Zhang, P.; Li, Y.; Wu, Z.; Zhao, Y.; Chai, Z. Quantifying the Biodistribution of Nanoparticles. *Nat. Nanotechnol.* **2011**, *6*, 755.

- (13) Dobrovolskaia, M. A.; McNeil, S. E. Immunological Properties of Engineered Nanomaterials. *Nat. Nanotechnol.* **2007**, *2*, 469–478.
- (14) Liang, L.; Li, J.; Li, Q.; Huang, Q.; Shi, J.; Yan, H.; Fan, C. Cover Picture: Single-Particle Tracking and Modulation of Cell Entry Pathways of a Tetrahedral DNA Nanostructure in Live Cells. *Angew. Chem., Int. Ed.* **2014**, *53*, 7745–7750.
- (15) Kreyling, W. G.; Fertsch-Gapp, S.; Schäffler, M.; Johnston, B. D.; Haberl, N.; Pfeiffer, C.; Diendorf, J.; Schleh, C.; Hirn, S.; Semmler-Behnke, M.; Epple, M.; Parak, W. J. *In Vitro* and *In Vivo* Interactions of Selected Nanoparticles with Rodent Serum Proteins and Their Consequences in Biokinetics. *Beilstein J. Nanotechnol.* **2014**, *5*, 1699–1711.
- (16) Hadjidemetriou, M.; Al-Ahmady, Z. S.; Kostarelos, K. Time-Evolution of *In Vivo* Protein Corona onto Blood-Circulating PEGylated Liposomal Doxorubicin (DOXIL) Nanoparticles. *Nanoscale* **2016**, *8*, 6948–6957.
- (17) Huang, K.; Ma, H.; Liu, J.; Huo, S.; Kumar, A.; Wei, T.; Zhang, X.; Jin, S.; Gan, Y.; Wang, P. C.; He, S.; Zhang, X.; Liang, X. J. Size-Dependent Localization and Penetration of Ultrasmall Gold Nanoparticles in Cancer Cells, Multicellular Spheroids, and Tumors *In Vivo*. *ACS Nano* **2012**, *6*, 4483–4493.
- (18) Chou, L. Y. T.; Zagorovsky, K.; Chan, W. C. DNA Assembly of Nanoparticle Superstructures for Controlled Biological Delivery and Elimination. *Nat. Nanotechnol.* **2014**, *9*, 148–155.
- (19) Blanco, E.; Shen, H.; Ferrari, M. Principles of Nanoparticle Design for Overcoming Biological Barriers to Drug Delivery. *Nat. Biotechnol.* **2015**, *33*, 941–951.
- (20) Irvine, D. J.; Hanson, M. C.; Rakhra, K.; Tokatlian, T. Synthetic Nanoparticles for Vaccines and Immunotherapy. *Chem. Rev.* **2015**, *115*, 11109–11146.
- (21) Veisheh, O.; Doloff, J. C.; Ma, M.; Vegas, A. J.; Tam, H. H.; Bader, A. R.; Li, J.; Langan, E.; Wyckoff, J.; Loo, W. S.; Jhunjhunwala, S.; Chiu, A.; Siebert, S.; Tang, K.; Hollister-Lock, J.; Aresta-Dasilva, S.; Bochenek, M.; Mendoza-Elias, J.; Wang, Y.; Qi, M.; et al. Size- and Shape-Dependent Foreign Body Immune Response to Materials Implanted in Rodents and Non-Human Primates. *Nat. Mater.* **2015**, *14*, 643–651.
- (22) Grassian, V. H.; Haes, A. J.; Mudunkotuwa, I. A.; Demokritou, P.; Kane, A. B.; Murphy, C. J.; Hutchison, J. E.; Isaacs, J. A.; Jun, Y. S.; Karn, B.; Khondaker, S. I.; Larsen, S. C.; Lau, B. L. T.; Pettibone, J. M.; Sadik, O. A.; Saleh, N. B.; Teague, C. NanoEHS - Defining Fundamental Science Needs: No Easy Feat When the Simple Itself Is Complex. *Environ. Sci.: Nano* **2016**, *3*, 15–27.
- (23) Hamad-Schifferli, K. Exploiting the Novel Properties of Protein Coronas: Emerging Applications in Nanomedicine. *Nanomedicine* **2015**, *10*, 1663–1674.
- (24) Malvindi, M. A.; Brunetti, V.; Vecchio, G.; Galeone, A.; Cingolani, R.; Pompa, P. P. SiO₂ Nanoparticles Biocompatibility and Their Potential for Gene Delivery and Silencing. *Nanoscale* **2012**, *4*, 486–495.
- (25) Sokolova, V.; Westendorf, A. M.; Buer, J.; Uberla, K.; Epple, M. The Potential of Nanoparticles for the Immunization Against Viral Infections. *J. Mater. Chem. B* **2015**, *3*, 4767–4779.
- (26) Zhang, Y. N.; Poon, W.; Tavares, A. J.; McGilvray, I. D.; Chan, W. C. Nanoparticle–Liver Interactions: Cellular Uptake and Hepatobiliary Elimination. *J. Controlled Release* **2016**, *240*, 332–348.
- (27) Hadjidemetriou, M.; Al-Ahmady, Z.; Mazza, M.; Collins, R. F.; Dawson, K. A.; Kostarelos, K. *In Vivo* Biomolecule Corona around Blood-Circulating, Clinically Used and Antibody-Targeted Lipid Bilayer Nanoscale Vesicles. *ACS Nano* **2015**, *9*, 8142–8156.
- (28) Walczyk, D.; Baldelli Bombelli, F.; Monopoli, M. P.; Lynch, I.; Dawson, K. A. What the Cell “Sees” in Bionanoscience. *J. Am. Chem. Soc.* **2010**, *132*, 5761–5768.
- (29) Walkey, C. D.; Olsen, J. B.; Song, F.; Liu, R.; Guo, H.; Olsen, D. W.; Cohen, Y.; Emili, A.; Chan, W. C. Protein Corona Fingerprinting Predicts the Cellular Interaction of Gold and Silver Nanoparticles. *ACS Nano* **2014**, *8*, 2439–2455.
- (30) Kelly, P. M.; Åberg, C.; Polo, E.; O’Connell, A.; Cookman, J.; Fallon, J.; Krpetić, Ž.; Dawson, K. A. Mapping Protein Binding Sites on the Biomolecular Corona of Nanoparticles. *Nat. Nanotechnol.* **2015**, *10*, 472–479.
- (31) Lo Giudice, M. C.; Herda, L. M.; Polo, E.; Dawson, K. A. *In Situ* Characterization of Nanoparticle Biomolecular Interactions in Complex Biological Media by Flow Cytometry. *Nat. Commun.* **2016**, *7*, 13475.
- (32) Huhn, J.; Fedeli, C.; Zhang, Q.; Masood, A.; del Pino, P.; Khashab, N. M.; Papini, E.; Parak, W. J. Dissociation Coefficients of Protein Adsorption to Nanoparticles as Quantitative Metrics for Description of the Protein Corona: A Comparison of Experimental Techniques and Methodological Relevance. *Int. J. Biochem. Cell Biol.* **2016**, *75*, 148–161.
- (33) Kumar, V.; Butcher, S. J.; Öörni, K.; Engelhardt, P.; Heikkonen, J.; Kaski, K.; Ala-Korpela, M.; Kovanen, P. T. Three-Dimensional CryoEM Reconstruction of Native LDL Particles to 16 Å Resolution at Physiological Body Temperature. *PLoS One* **2011**, *6*, e18841.
- (34) Mora, S.; Szklo, M.; Otvos, J. D.; Greenland, P.; Psaty, B. M.; Goff, D. C., Jr.; O’Leary, D. H.; Saad, M. F.; Tsai, M. Y.; Sharrett, A. R. LDL Particle Subclasses, LDL Particle Size, and Carotid Atherosclerosis in the Multi-Ethnic Study of Atherosclerosis (MESA). *Atherosclerosis* **2007**, *192*, 211–217.
- (35) Segrest, J. P.; Jones, M. K.; De Loof, H.; Dashti, N. Structure of Apolipoprotein B-100 in Low Density Lipoproteins. *J. Lipid Res.* **2001**, *42*, 1346–1367.
- (36) Hansel, T. T.; Kropshofer, H.; Singer, T.; Mitchell, J. A.; George, A. J. T. The Safety and Side Effects of Monoclonal Antibodies. *Nat. Rev. Drug Discovery* **2010**, *9*, 325–338.
- (37) Herda, L. M.; Hristov, D. R.; Lo Giudice, M. C.; Polo, E.; Dawson, K. A. Mapping of Molecular Structure of the Nanoscale Surface in Bionanoparticles. *J. Am. Chem. Soc.* **2017**, *139*, 111–114.
- (38) Resch-Genger, U.; Grabolle, M.; Cavaliere-Jaricot, S.; Nitschke, R.; Nann, T. Quantum Dots *Versus* Organic Dyes as Fluorescent Labels. *Nat. Methods* **2008**, *5*, 763–775.
- (39) Zarschler, K.; Prapainop, K.; Mahon, E.; Rocks, L.; Bramini, M.; Kelly, P. M.; Stephan, H.; Dawson, K. A. Diagnostic Nanoparticle Targeting of the EGF-Receptor in Complex Biological Conditions Using Single-Domain Antibodies. *Nanoscale* **2014**, *6*, 6046–6056.
- (40) Levitan, I.; Volkov, S.; Subbaiah, P. V. Oxidized LDL: Diversity, Patterns of Recognition, and Pathophysiology. *Antioxid. Redox Signaling* **2010**, *13*, 39–75.
- (41) Brown, M. S.; Goldstein, J. L. Reversible Accumulation of Cholesteryl Esters in Macrophages Incubated with Acetylated Lipoproteins. *J. Cell Biol.* **1979**, *82*, 597–613.
- (42) Karsten, C. M.; Köhl, J. The Immunoglobulin, IgG Fc Receptor and Complement Triangle in Autoimmune Diseases. *Immunobiology* **2012**, *217*, 1067–1079.
- (43) Lund, J.; Winter, G.; Jones, P. T.; Pound, J. D.; Tanaka, T.; Walker, M. R.; Artymiuik, P. J.; Arata, Y.; Burton, D. R.; Jefferis, R.; Woof, J. M. Human Fc Gamma RI and Fc Gamma RII Interact with Distinct but Overlapping Sites on Human IgG. *J. Immunol.* **1991**, *147*, 2657–2662.
- (44) Canfield, S. M.; Morrison, S. L. The Binding Affinity of Human IgG for Its High Affinity Fc Receptor Is Determined by Multiple Amino Acids in the CH2 Domain and Is Modulated by the Hinge Region. *J. Exp. Med.* **1991**, *173*, 1483–1491.
- (45) Mahon, E.; Hristov, D. R.; Dawson, K. A. Stabilising Fluorescent Silica Nanoparticles against Dissolution Effects for Biological Studies. *Chem. Commun.* **2012**, *48*, 7970–7972.
- (46) Piella, J.; Bastús, N. G.; Puentes, V. Size-Controlled Synthesis of Sub-10-Nanometer Citrate-Stabilized Gold Nanoparticles and Related Optical Properties. *Chem. Mater.* **2016**, *28*, 1066–1075.
- (47) Gallo, J.; García, I.; Genicio, N.; Penadés, S. CdTe-Based QDs: Preparation, Cytotoxicity, and Tumor Cell Death by Targeting Transferrin Receptor. *Part. Part. Syst. Character.* **2014**, *31*, 126–133.